Slowing-down time of energetic atoms in solids

Mark T. Robinson
Solid State Division, Oak Ridge National Laboratory, Post Office Box 2008, Oak Ridge, Tennessee 37831-6032
(Received 22 March 1989)

Computer simulation models for the slowing down of energetic atoms in matter are often based on the binary collision approximation (BCA). Such models typically ignore the temporal aspects of the problem. A method is described whereby calculations of the times at which energetic particles reach their collision points may be included in such BCA simulations without altering the "event-driven" structure of the model. The enhanced model is illustrated by calculations of the time required by 10-eV to 10-keV Cu atoms to slow down in both crystalline and amorphous Cu targets. In addition to the mean slowing-down time, distributions of slowing-down times and correlations between slowing-down times and particle ranges are presented. The utility of range-time correlations in studying penetration problems is demonstrated.

I. INTRODUCTION

Computer simulation is a well-established method for studying the slowing down of fast atomic particles in solids, the resulting defect distributions, and such consequences as particle reflection and target sputtering (for reviews, see Refs. 1–4). Ideally, these calculations are based on classical dynamical models in which the equations of motion of many mutually interacting particles are solved for appropriate initial and boundary conditions, but even with modern computers, they are limited to small samples of primary particles of modest initial kinetic energy and to solids with such symmetrical structures as close-packed or nearly close-packed metals. While progress is being made in extending the limits of such calculations,[5,6] approximate methods must still be used to simulate the slowing down of high-energy particles in complex crystalline media or in noncrystalline ones. This is especially true if sufficient statistical accuracy is needed to interpret experiments.

The binary collision approximation (BCA) facilitates atomic slowing-down calculations. Each particle trajectory is constructed as a series of two-body encounters with initially stationary target atoms. An approximate treatment can be given of the nearly simultaneous encounter of a projectile with several target atoms. Target structures are unlimited, since it is feasible to include many material regions, each with an arbitrary (triclinic) crystal structure containing many kinds of atoms, or to simulate noncrystalline media using aleatory methods. However, BCA models generally proceed from collision to collision without explicit reference to the time: they are "event driven", in Harrison's phrase.[2] They cannot, therefore, include collisions between moving particles or be used to study correlations in cascade development where knowledge of the time is essential.

The purpose of this paper is to show how time can be included explicitly in BCA calculations and how the temporal aspects of particle trajectories may be studied without abandoning the event-driven structure of the model. This is accomplished by computing the time at which each projectile reaches each of its collision points, with appropriate corrections for its changes in velocity as it approaches and departs from each such point in its trajectory. The calculation is exact for strictly binary encounters in which the collision partners are truly isolated from other particles. Yamamura[7] has reported calculations with a time-dependent binary collision program, but his model has not been described in detail.

The calculations reported here were made with an extensively modified version of the MARLOWE code.[1,8–12] Besides introducing the time evaluations, it was necessary to make substantial changes in the selection of target sites, as will subsequently be described. The methods of evaluating the scattering integrals and of propagating the target crystal were described earlier.[8,11,12] In addition to illustrating a time-resolved BCA model, the calculations reported below show the general utility of evaluating the temporal data, even in rather simple particle-range calculations. The interpretation of the results is made much easier by the availability of such information.

II. THE COMPUTATIONAL MODEL

A. Two body elastic scattering

Time may be introduced into the BCA by using the constant velocity of the center-of-mass in each binary encounter to clock that event. Consider the situation sketched in Fig. 1. A projectile of mass m_1 and initial kinetic energy E_0 is located at a point P_0 at a time which is taken as the origin of the (local) time coordinate. A target atom of mass m_2 is initially at rest at the point T_0, the origin of the (local) space coordinates. The mass ratio $A = m_2/m_1$. The points P_0 and T_0 are separated by a distance L, sufficiently large that interactions between the two particles may be neglected. The impact parameter p, the barycentric scattering angle θ, the time integral τ, and the laboratory scattering angles ϑ and ϕ are defined in Fig. 1, which shows the two particles and their barycenter at the apsis in the collision. The barycenter continues moving to the right until the scattered particles

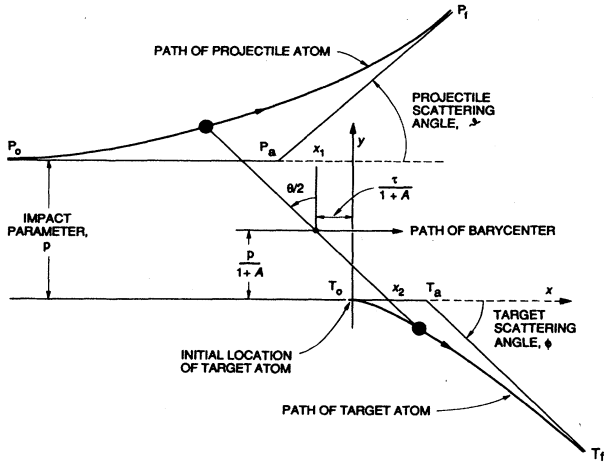

FIG. 1. The trajectories of a projectile and an initially stationary target atom interacting according to a conservative central repulsive force. The positions of the particles and of their barycenter are shown at the apsis of the encounter.

reach the points P_f and T_f, respectively, also separated by the distance L, beyond which interactions are ignored.

The model uses a "quasielastic" approximation in which a "local" inelastic (electron excitation) energy loss Q occurs at the apsis in an encounter, a loss taken from the kinetic energy of the barycenter. Consequently, the time for the second part of the encounter is increased by a factor $1/f$, where

$$f=[1-(1+A)Q/AE_0]^{1/2} .$$

The laboratory scattering angles are related to those in the barycentric system by

$$\tan\vartheta = Af\sin\theta/(1+Af\cos\theta) ,$$
$$\tan\phi = f\sin\theta/(1-f\cos\theta) . \quad (1)$$

The laboratory asymptotes intersect in the points P_a and T_a, found by computing the magnitudes x_1 and x_2 shown in Fig. 1:

$$x_1=[(1+f)\tau+(fA-1)p\tan(\theta/2)]/f(1+A) , \quad (2)$$
$$x_2=p\tan(\theta/2)-x_1 . \quad (3)$$

The latter is the length of the incoming asymptote to the target trajectory. The length of the incoming asymptote to the projectile trajectory is $\hat{\zeta}=\zeta-x_1$, where $\zeta=(L^2-p^2)^{1/2}$.

Solution of the classical equations of motion[13] allows the barycentric scattering angle and the so-called time integral[14] to be expressed as

$$\theta=\pi-2p\int_R^\infty dr[r^2g(r)]^{-1} , \quad (4)$$
$$\tau=(R^2-p^2)^{1/2}-\int_R^\infty dr\{[g(r)]^{-1}-(1-p^2/r^2)^{-1/2}\}, \quad (5)$$

where

$$g(r)=[1-p^2/r^2-(1+A)V(r)/AE]^{1/2} ,$$

r is the interatomic separation, $V(r)$ is the interatomic potential energy function, and R is the apsis in the collision, defined by $g(R)=0$. The inelastic energy loss is ignored in the barycentric scattering integrals, hence the description "quasielastic." The integral τ is the difference between the time taken by a noninteracting projectile to reach its apsis with the target and that taken by a scattered particle, scaled by the initial velocity of the projectile, $v_0=(2E_0/m_1)^{1/2}$. The numerical evaluation of the integrals (4) and (5) is discussed elsewhere.[8,15]

As the two particles move from P_0,T_0 to the apsis, their barycenter moves a distance $(\zeta-\tau)/(1+A)$ at a velocity $v_0/(1+A)$ in the time $(\zeta-\tau)/v_0$. If the collision were strictly elastic, the particles would take the same time to move on to the points P_f, and T_f, but the local inelastic energy loss increases this by a factor $1/f$. The calculation of the coordinates of P_a and T_a accounts for the slowing down of the projectile and the initial acceleration of the target. The time assigned to the particles at P_a,T_a must also allow for the acceleration of the atoms as they leave the apsis. The length of the outgoing asymptote to the projectile trajectory from P_a to P_f is evaluated and then the time to traverse it taken by a particle with the constant velocity $v_1=(2E_1/m_1)^{1/2}$, where

$$E_1=[(1-fA)^2+4fA\cos^2(\theta/2)]E_0/(1+A)^2$$

is the final projectile kinetic energy. A similar calculation of the length of the outgoing asymptote to the target trajectory from T_a to T_f and the time to traverse it by a particle with the velocity $v_2=(2E_2/m_2)^{1/2}$, where

$$E_2=[(1-f)^2A+4fA\sin^2(\theta/2)]E_0/(1+A)^2 \quad (6)$$

is the final target kinetic energy, gives the same result, namely

$$\zeta^*=v_0t_a=\zeta+(1/f)[p\tan(\theta/2)-(1+f)\tau] , \quad (7)$$

where t_a is the time assigned to both particles at the apsis.

In addition to the local inelastic energy loss, the model includes a "nonlocal" loss which depends on the distance traversed by the projectile. The time calculated in Eq. (7) must be adjusted to reflect the slowing down of the projectile associated with this loss by multiplying t_a by the factor $-(1/q)\ln(1-q)$, where $q=kE_0^{1/2}\hat{\zeta}/2E_0$ and the factor $kE_0^{1/2}$ is the nonlocal inelastic stopping power.

B. The selection of target atoms

The method used to select appropriate target atoms and to treat the nearly simultaneous encounter of a projectile with several targets is illustrated by Fig. 2. A projectile located at the point P moves along the unit vector $\boldsymbol{\lambda}_0$. Target atoms are located at the points T_1 and T_2, generated as described previously.[8,11] The vector from the projectile to the ith target is $\Delta\mathbf{x}_i$ (only that to T_1 is shown). The distance along $\boldsymbol{\lambda}_0$ to the point nearest a target is $\zeta_i=\boldsymbol{\lambda}_0\cdot\Delta\mathbf{x}_i$ and the impact parameter is $p_i^2=(\boldsymbol{\lambda}_0\times\Delta\mathbf{x}_i)^2$. Targets are accepted if $p_i\le p_c$ and $\zeta_i>\zeta_{\min}$. The value of $\zeta_{\min}$ was set in the previous collision of the projectile (see below) and p_c is chosen to be

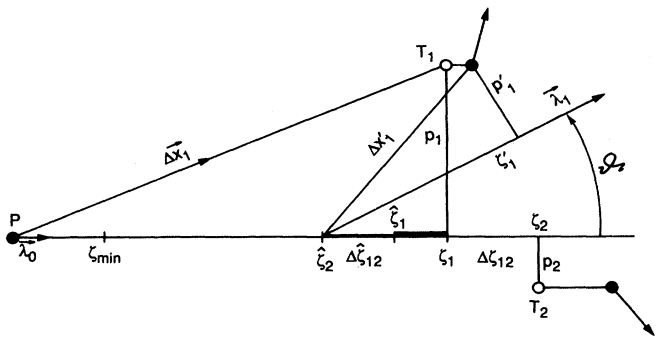

FIG. 2. The selection of target atoms and the treatment of nearly simultaneous collisions. See the text for an explanation.

somewhat less than the nearest neighbor distance in the target crystal.

Originally,[8] the distance to the first collision point along λ_0 was determined: This is ζ_1 in the sketch. Other target atoms were considered only if they met the criterion $\Delta\zeta_{fi}=\zeta_i-\zeta_f<\Delta\zeta_{\max}$, where the subscript f refers to the first target and $\Delta\zeta_{\max}$ was usually 50 pm. This criterion ignores the effects of the time integral on the position of a collision point: At low energies, the time integral is comparable to interatomic distances and may even change the order of collision points, as shown schematically in Fig. 2. When this happens in the original model, particles may move backwards to a collision point. Such negative motions have only minor effects on projectile ranges and other spatial aspects of trajectories, but the effects on the time values are profound: some projectiles even had negative slowing down times, a physically absurd result. To correct this situation, all targets generated by the crystal propagation procedure are accepted as long as $\zeta_i>\zeta_{\min}$ and $p_i\le p_c$. Consequently, more scattering integrals are evaluated than before.

At this point in the calculation, it is determined whether or not the selected lattice sites are occupied by atoms, a step guaranteeing that particle number is conserved and that no lattice site emits more than a single projectile.

After the asymptote intersections are located, the first one along λ_0 is found. Targets are retained as long as $\Delta\hat{\zeta}_{fi}=\hat{\zeta}_i-\hat{\zeta}_f<\Delta\hat{\zeta}_{\max}$, where the subscript f refers to the first asymptote intersection. The limit $\Delta\hat{\zeta}_{\max}$ is usually taken as 25 pm. In addition, it is required in the modified model that ζ_f^* exceed a minimum value $\Delta\zeta^*_{\min}$, usually taken as zero. The last condition prevents negative time increments from occurring in the calculation. The code keeps track of targets rejected for failing this condition: the frequency and nature of such events are discussed later.

C. Nearly simultaneous collisions

After the scattering integrals are evaluated for each encounter deemed by the above procedures to occur at the same time, the results are combined into a whole almost as described before.[9] The direction and kinetic energy of each target atom are evaluated as if it alone were involved in a collision with the projectile, using Eqs. (1), (3), and (6). The direction and momentum of the scattered projectile are evaluated by applying the conservation of linear momentum to the incident projectile momentum and the set of target momenta. Finally, the conservation of energy is used to scale the momenta of all particles. The algorithm is exact when there is only one target, but generally underestimates the energy transferred to multiple targets.

The local inelastic energy loss is considered in the kinematics of each contributing partial collision, but the nonlocal inelastic loss is not. Thus, it is possible for the sum of the kinetic energies of the emerging particles and the inelastic energy loss to exceed the kinetic energy of the incoming projectile. When this situation occurs, the projectile kinetic energy is set to zero; the inelastic energy loss and the target particle kinetic energies are scaled equally to assure energy conservation.

Each target atom is placed at the intersection of its laboratory asymptotes, a distance x_2 from its initial position. The projectile is placed at $\hat{\zeta}_f$, the first asymptote intersection along λ_0. This differs slightly from earlier practice, where the mean $\hat{\zeta}_i$ value was used. The difference is small and has only a small effect on the spatial results. The new position is probably somewhat more plausible than was the earlier one. The time associated with the collision is obtained from Eq. (7) for the scattering event which determines the projectile position. This value is assigned to each of the particles emerging from the event.

D. Preparing for the next collision

At the completion of each collision, the parameters which control the next collision of the projectile are established. The method is sketched in fig. 2. The direction of the projectile after scattering is λ_1, which makes an angle ϑ with λ_0. For each target atom, the distance forward along λ_1 is $\zeta_i'=\lambda_1\cdot\Delta\mathbf{x}_i'$ (only that to T_1 is shown) and the impact parameter is $(p_i')^2=(\lambda_1\times\Delta\mathbf{x}_i)^2$. Originally,[8] the value of $\zeta_{\min}$ for the next encounter of the projectile was set to the greatest value of ζ_i' for any target, subject to a minimum, usually 25 pm. This scheme guaranteed that no target was encountered again in the next collision of the projectile.

It is easily shown that in binary encounters, $p'>p$, but if there are multiple targets as in Fig. 2, usually some will have $p_i'<p_i$. This is especially true when large projectile deflections occur. In such situations it may be more realistic to allow a further collision with a closely approached target. Consequently, in the modified model, if $\vartheta>\vartheta_{\min}$, targets with $p_i'<p_i$ are excluded from the determination of $\zeta_{\min}$. Both the spatial and the temporal aspects of projectile trajectories are fairly insensitive to the value of $\vartheta_{\min}$. The value $\pi/4$ (45°) was chosen, since it minimized the number of targets rejected for inducing negative time increments.

III. PRIMARY SLOWING-DOWN CALCULATIONS

The model described above is illustrated by a series of calculations on the slowing down of 10-eV to 10-keV Cu

atoms in Cu targets, calculations of a type that have often been made before.[8,14] Besides the usual range calculations, the times required for the particles to slow down were evaluated as well as correlations between the ranges and the slowing-down times.

A. Computational parameters

The interactions of the atoms were governed by the Molière potential with the screening length $a_{12}=7.38$ pm.[8] The lattice constant of Cu was $a_0=0.3615$ nm and the impact parameters were cut off at $p_c/a_0=0.62$. The inelastic energy losses were taken from the LSS theory.[16] Four-point Gauss-Mehler quadrature was used to evaluate the scattering integrals. The targets were often static single crystals. For polycrystalline targets, the crystal axes were rotated randomly and isotropically about a lattice site close to the primary impact point before launching each primary. For "amorphous" targets, a similar rotation about a lattice site near the projectile position was performed before each collision. The projectiles were followed until their kinetic energies fell below a value E_c, usually 5 eV. Sets of 10 000 primary particles were generated with randomly selected initial conditions: directions of motion for particles starting from lattice sites; impact points for particles entering a crystal surface from outside. Distributions were recorded of the time taken by the projectiles to slow down and of various components of their ranges. Several central measures of these distributions were recorded. The resulting mean ranges and slowing-down times were evaluated with a precision of about 1%.

The calculation were done on a Data General Corporation Eclipse MV/10 000^{TM} computer. A calculation for projectiles launched from lattice sites at 10 keV required about 48 min to perform; times were roughly proportional to the initial projectile velocity. Calculations for projectiles launched from outside the target required much longer times because of channeling: 2 h for 10-keV projectiles incident on a polycrystalline target.

The results reported here emphasize the *radial range* and the *slowing-time*. The radial range, also called the "vector" range,[8–11,14] is the distance from the initial site of the particle to its final collision point. The slowing-down time is the difference between the time at which the particle makes its final collision and the time at which it began to move. A few results are also reported for the *penetration*, the projection of the radial range onto the initial direction of the primary.

B. Rejection of target atoms

As mentioned before, difficulties were encountered with time calculations using the original model[8–12] because negative particle motions resulted from collisions misordered in time by time-integral effects, but changes in the model eliminated most such events. A detailed investigation was made of the frequency and the nature of those remaining events in which targets were rejected because they would cause negative motion of a projectile.

Whatever the initial energy, such events occurred only near the end of a trajectory, usually in one of the last two or three collisions. As a result, their frequency depended strongly on the value of E_c. Furthermore, the rejected atom had always been a target in an earlier collision, usually two or three before the one in which the rejection occurred. In the earlier collision, the target often received enough energy from the projectile to be regarded as displaced had cascades been generated. In that case, the later target rejection would not have occurred since its site would then be unoccupied. The incidence of such events was always low: at initial energies above 100 eV, only one trajectory in five involved rejected targets, rarely more than one each. At lower energies, lattice effects increased the incidence of rejection to as many as one trajectory in three, but other aspects of the situation were unchanged. If thermal displacements or random rotations were included in the model, more targets were rejected because these processes often put atoms in locations inconsistent with the previous history of the projectile: for example, an atom could be rotated into a position just in front of a projectile where it would compel negative motion. The rejection of targets eliminates collisions with such particles, as well as inappropriate repeat encounters.

In no case did such target rejection influence either the spatial or the temporal aspects of the trajectories to a significant extent. Statistical uncertainties springing from altogether other causes were always far greater than any effect of the rejection of a few target atoms.

C. Effects of the cut-off energy, E_c

It is well known that the ranges of energetic atoms in solids are dominated by their initial kinetic energies and that the choice of cutoff energy has relatively little effect on the results of range calculations. Figure 3 shows the mean radial ranges and slowing-down times of Cu atoms recoiling from lattice sites in a static Cu monocrystal as functions of E_c, normalized to the values for $E_c=5$ eV, for three initial kinetic energies. The radial range is relatively insensitive to the choice of cutoff: At 10 keV, an order-of-magnitude change in E_c produces a change in the mean radial range of only 2%. The sensitivity increases when the cutoff energy becomes a significant fraction of the initial energy, but these results show that the ranges of the particles are determined primarily by the early portions of their trajectories, as expected.

This behavior contrasts with that of the slowing-down time which shows a substantial dependence on the final energy chosen. In fact, the slowing-down times are dominated by the late portions of the trajectories, where the projectiles are moving most slowly, and must be sensitive to low-energy aspects of the model. Comparisons between BCA slowing-down time calculations and either experiments (currently not feasible) or other calculations requires careful attention to the final energies involved.

D. Final-energy distributions

Distributions of the final projectile kinetic energy E_f are shown in Fig. 4 for 10 keV projectiles slowing down in Cu for several variations in the model. The effect of varying E_c in the nonlocal inelastic loss model is shown

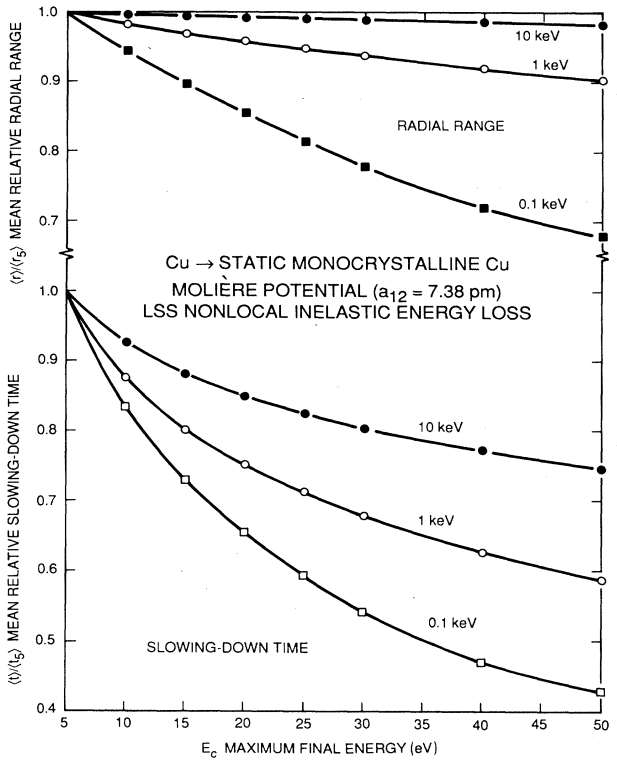

FIG. 3. The mean radial range and the mean slowing-down time of Cu atoms recoiling from lattice sites in static monocrystalline Cu, as functions of the cutoff energy E_c, normalized to the values for $E_c = 5$ eV.

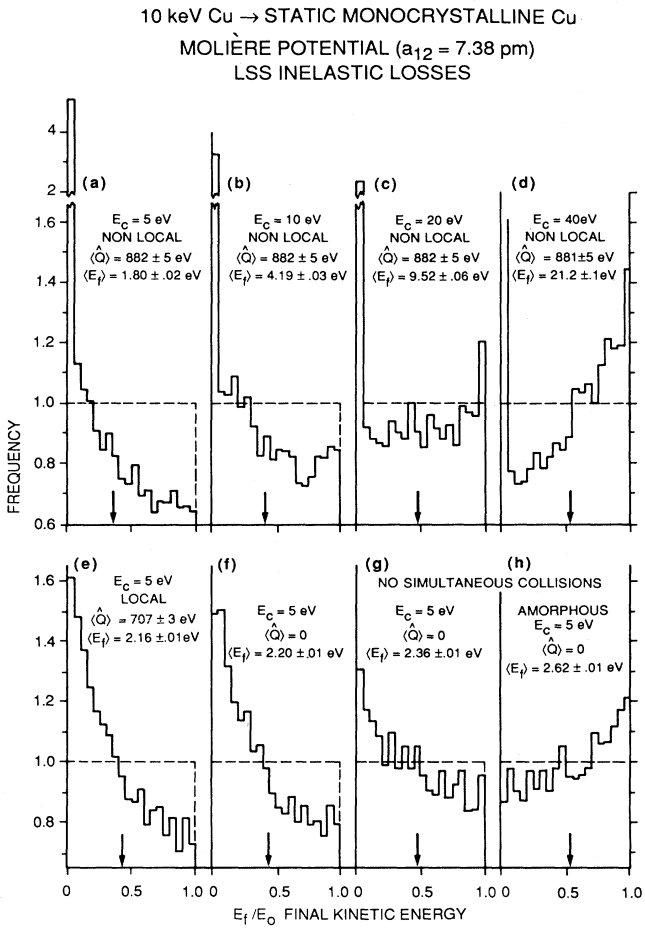

FIG. 4. The final energy spectra of 10-keV Cu atoms recoiling from lattice sites in static monocrystalline Cu. The arrows mark the mean final energy $\langle E_f \rangle$. The effects of several variations in the model are shown.

in parts (a) through (d). In each case, a large peak near $E_f = 0$ results from the energy scaling performed when the sum of the indicated elastic and inelastic energy losses exceeds the kinetic energy with which a projectile enters a collision. The mean total inelastic energy loss $\langle \hat{Q} \rangle$ is essentially independent of E_f, but some 10% to 25% of the projectiles require the rescaling of their energy losses, a fraction that decreases as E_c increases.

When the local inelastic energy loss model is used, such rescaling is rarely necessary, even at $E_c = 5$ eV, and the peak near $E_f = 0$ is greatly reduced, as Fig. 4(e) shows. The final-energy spectrum obtained with the local model differs but slightly from that obtained in Fig. 4(f) with no inelastic energy losses at all. The shape of the spectra in these cases results from the effects of simultaneous collisions on the final energies. This can be seen from Fig. 4(g), which shows calculations performed with neither inelastic energy losses nor simultaneous collisions.

The shape of this spectrum is still not what might be expected, since small-angle scattering is much more probable than large-angle scattering, just the opposite of what the figure implies. The calculation was repeated for an amorphous target, with the result shown in Fig. 4(h). The final-energy spectrum for the amorphous medium shows the expected preference for small-angle elastic scattering. This spectral shape gradually appears in the nonlocal inelastic loss results when E_c is increased sufficiently. Thus, the crystallinity of the target influences the final energy spectrum (and therefore the slowing-down time), in addition to the cutoff energy, the model used for the inelastic energy losses, and the presence of simultaneous collisions.

IV. SLOWING-DOWN TIMES IN CRYSTALLINE TARGETS

Figure 5 shows the mean radial range computed for 10-eV to 10-keV Cu atoms recoiling from lattice sites in static monocrystalline Cu targets and the corresponding mean time taken by the projectiles to slow down from their initial energies to < 5 eV, using the nonlocal inelastic energy loss model. These curves show several features which can be explained by reference to distributions of the radial range and the slowing-down time.

A. Low-energy slowing-down times and radial ranges

The step in the slowing-down time curve of Fig. 5 at about 18 eV can be understood by examining the slowing-down time and radial range distributions shown in Fig. 6. There is a close correspondence between the

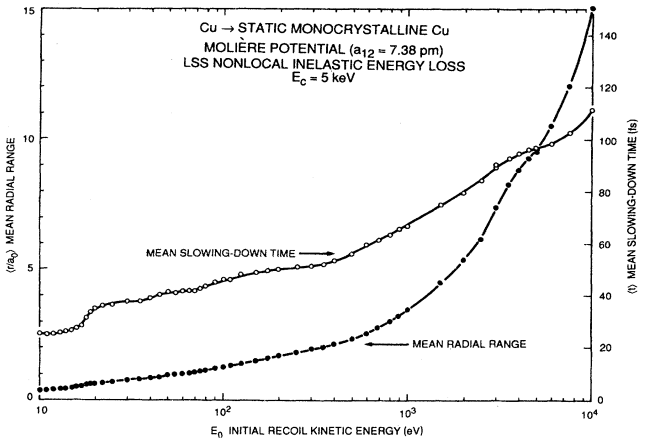

FIG. 5. The mean slowing-down time and the mean radial range for Cu atoms recoiling from lattice sites in static monocrystalline Cu.

time and the range histograms: The same groups of particles occur in both with the same number of particles in each group. The group positions in range change only slightly as the energy increases from 10 to 22 eV. The groups evidently represent particles stopped primarily by encounters with their near neighbors: up to 22 eV, only the first three groups of neighbors are important. In units of a_0, the distances from the initial primary site to these neighbors are 0.707, 1, and 1.225, respectively, but the distances to the actual collision points are reduced, partly by the quantity x_1 [see Fig. 1 and Eq. (2)] and partly by geometrical effects. The group positions are about 0.37, 0.68, and 0.88, respectively. The difference from the crystallographic values, averaging 0.33, is consistent with the scattering integrals appropriate to collisions at these low energies.

The group positions in time, in contrast, are not fixed, but move to smaller times as the particle velocities increase. The mean slowing-down times represent a balance between this effect and the changing populations of the groups. The mean time increases only slowly with the initial recoil energy from 10 to about 16 eV, where the third particle group first appears. It rises rapidly as this group grows in importance, but then grows more slowly until a fourth group appears at about 30 eV. Thus, the "waves" in the slowing-down time curve of Fig. 5 occur when the primaries are able to escape beyond particular sets of neighbors: Second neighbors at about 18 eV, third neighbors at about 40 eV, and so on. This behavior damps out as the energy reaches 100 eV or so, because so many different particle groups are involved. The 18 eV step may be related to the fact that the minimum displacement threshold in Cu is approximately 19 eV,[17] since only particles that leave the vicinity of their near neighbors are in fact permanently displaced. The "waves" are much less evident in the range curve, since the group positions in range are fixed and the mean

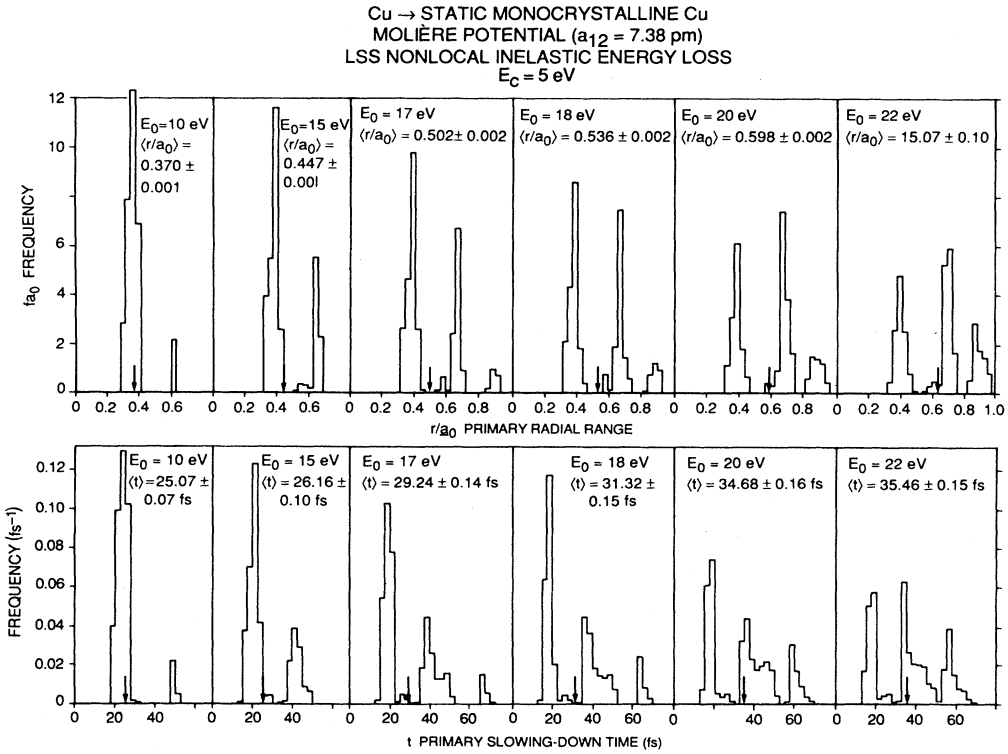

FIG. 6. Radial range and slowing-down time distributions for low-energy Cu atoms recoiling from lattice sites in static monocrystalline Cu. The arrows mark the mean values in each distribution.

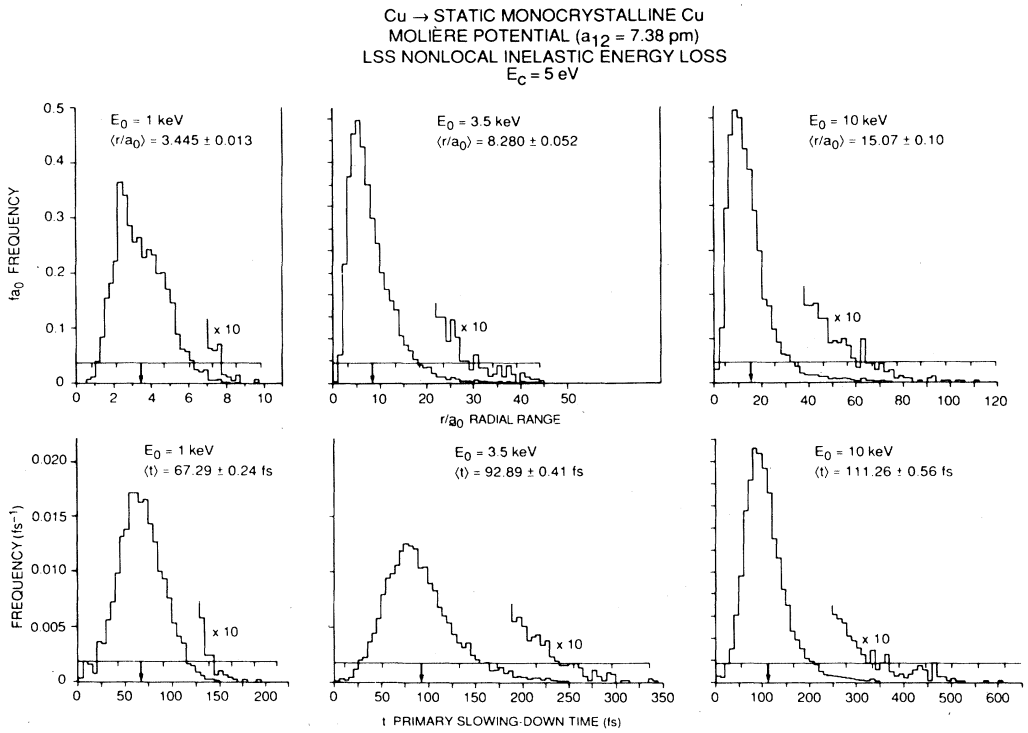

FIG. 7. Radial range and slowing-down time distributions for Cu atoms recoiling from lattice sites in static monocrystalline Cu. The arrows mark the mean values in each distribution. The scale above each arrow is marked in units of the standard deviation of the distribution.

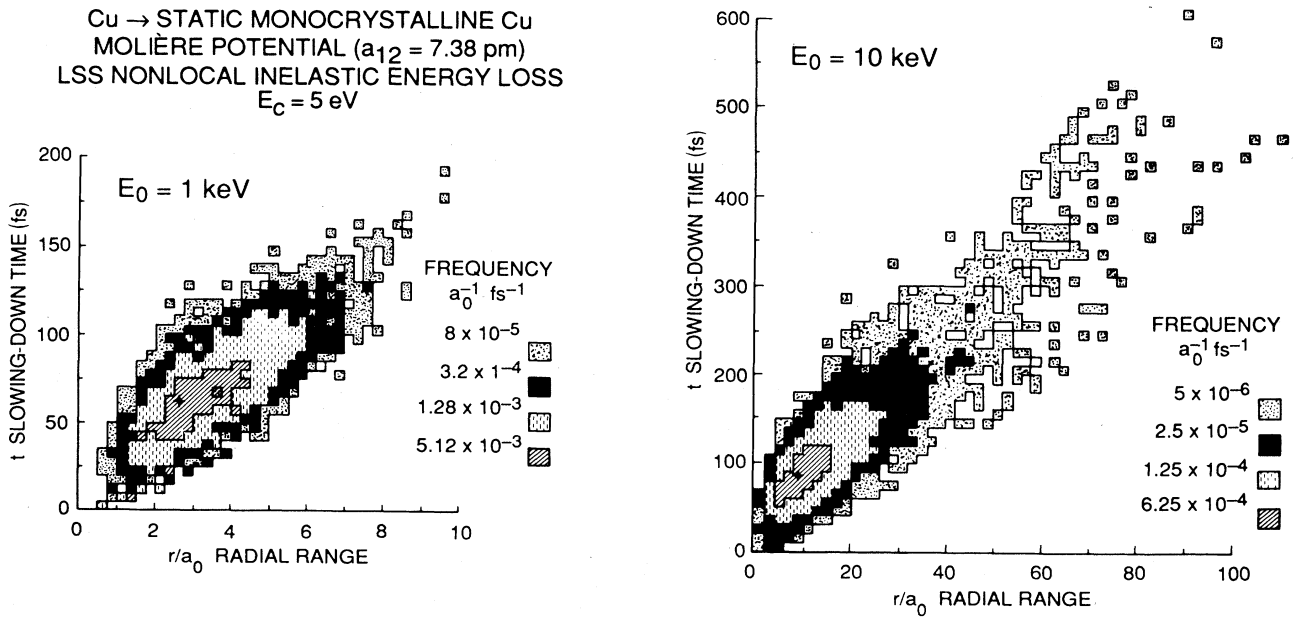

FIG. 8. Joint radial-range and slowing-down time distributions for 1- and 10-keV Cu atoms recoiling from lattice sites in static monocrystalline Cu. The + signs mark the maxima in the distributions. Four ranges of frequency are shown by the shading.

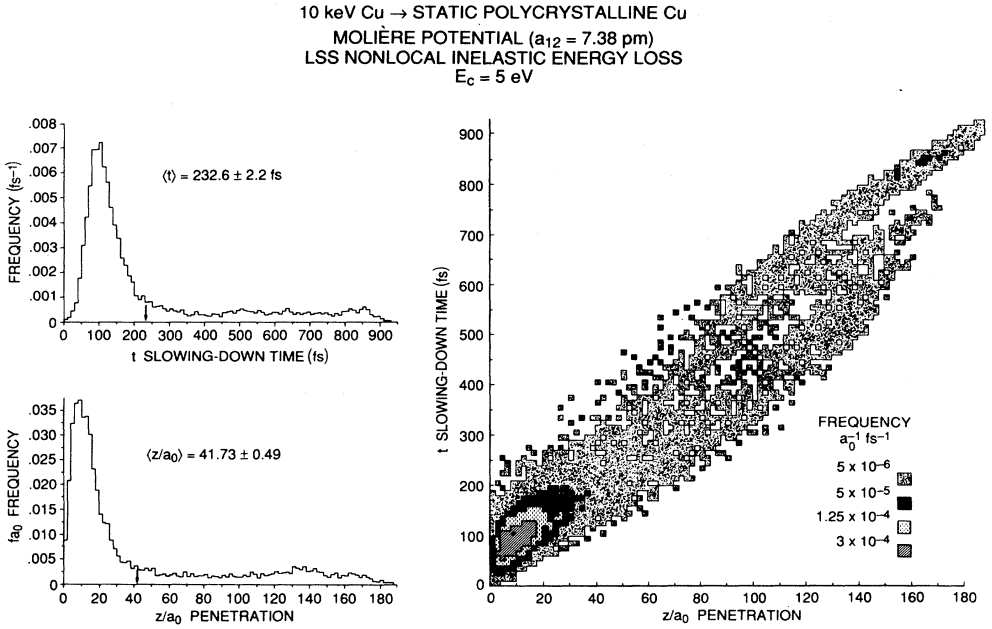

FIG. 9. Penetration and slowing-down time distributions for 10-keV Cu atoms at normal incidence upon polycrystalline Cu. The arrows mark the mean values in the two single-variable distributions. The + marks the maximum in the joint distribution. Four frequency ranges are shown by the shading.

radial range is determined only by the changing group populations.

B. Slowing-down times and radial ranges at higher energies

At higher energies, the local crystal structure no longer dominates the radial range and slowing-down time distributions. Distributions calculated at 1, 3.5, and 10 keV are shown in Fig. 7. The nearest-neighbor peak in the slowing-down time is still observable at 1 keV, but disappears at higher energies. As the initial kinetic energy increases, the distributions become increasingly skewed to the right, evidence that channeling is becoming important. The penetrating tail of the range distribution is hardly noticeable at 1 keV, but the quite unsymmetrical distribution suggests that at least a tendency towards channeling is beginning. Blocking of the primaries by neighboring atoms also contributes to the shape of this distribution. The development of a group of channeled particles and their increasing importance accounts for the somewhat sigmoid character of the curves in Fig. 5 near 4 keV.

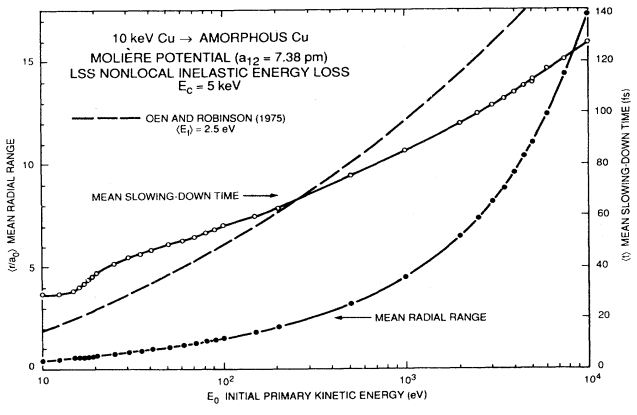

FIG. 10. The mean slowing-down time and the mean radial range for Cu atoms recoiling in amorphous Cu. The dashed line shows the slowing-down time calculated in a continuous slowing-down approximation.[18]

The slowing-down time distributions parallel the radial range distributions but are significantly less skewed. In addition to the less pronounced tail on the long-time side, they rise less abruptly on the short-time side than do the corresponding range distributions.

C. Correlations of radial ranges and slowing-down times

Correlations between the radial range and the slowing-down time were also investigated: Two examples are shown in Fig. 8. In general, of course, particles which stop slowly will travel greater distances than those which stop quickly. However, especially for intermediate ranges, there are so many possible trajectories that can lead to a particular range that considerable dispersion of the slowing-down times must be expected for most particles. This expectation is borne out in Fig. 8. At both energies, the slowing-down times and radial ranges are strongly correlated, but significant dispersion also occurs.

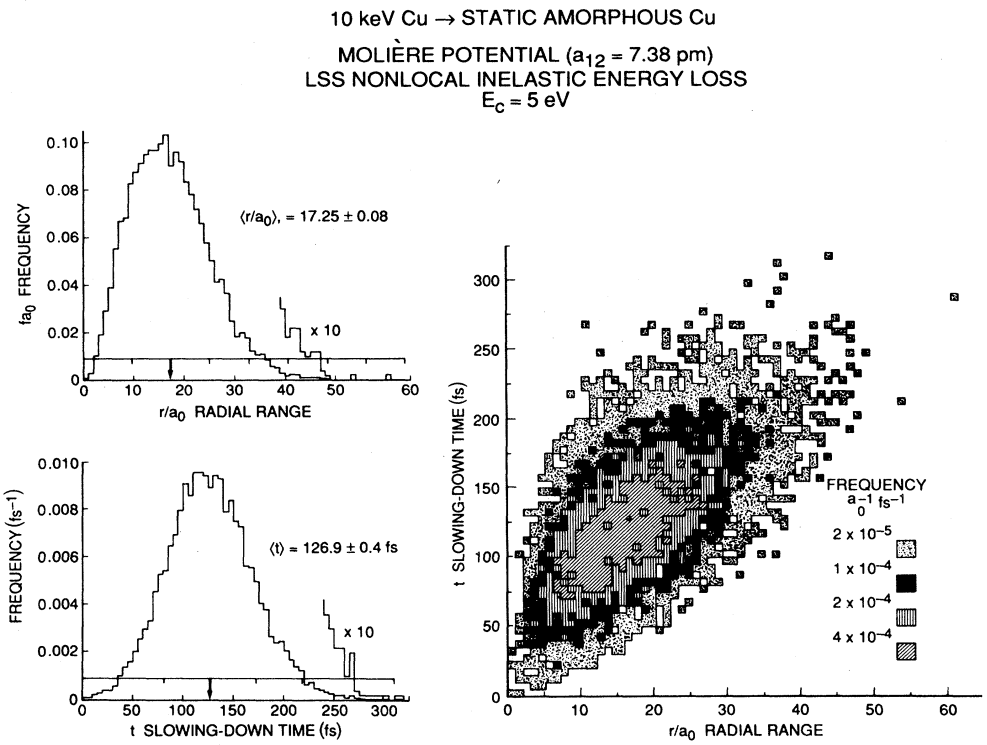

FIG. 11. Radial range and slowing-down time distributions for 10-keV Cu atoms recoiling from lattice sites in amorphous Cu. The arrows mark the mean values in the two single-variable distributions. The scale above each arrow is marked off in units of the standard deviation of the distribution. The + marks the maximum in the joint distribution. Four frequency ranges are shown by the shading.

At 10 keV, a pronounced tail extending to long ranges and long times represents the channeled particles. This tail is not significant at the lower energy.

Channeling is much more important for primaries injected into a crystalline target from outside. Figure 9 shows some results obtained for the penetration of 10-keV Cu atoms normally incident on a polycrystalline Cu target. Both the slowing-down time and the penetration distribution show the long persistent tail characteristic of channeling.[14] The joint distribution shows a pronounced tail region with an interesting structure. Therre is evidence of at least three particle groups, each with its own relationship between penetration and slowing-down time. These groups presumably represent the most open axial and planar channels in the fcc Cu crystal. Traces of this structure are probably present in Fig. 8 as well, but the much lower incidence of channeling for primaries recoiling from lattice sites obscures this point.

V. SLOWING-DOWN TIMES IN AMORPHOUS TARGETS

Figure 10 displays the results of some calculations of the mean slowing-down times and radial ranges of projectiles recoiling from initial sites in amorphous Cu targets. The amorphous model used is based on rotational disorder of the crystalline lattice, with preservation of the distances to near neighbors, and shows considerable short-range order. The mean slowing-down time in Fig. 10 shows the presence of the short-range order in the step near 18 eV, less abrupt than in the crystalline case of Fig. 5, but explained in the same way. No other structure remains in either the slowing-down time or the radial range curves.

The slowing-down times evaluated for amorphous Cu targets may be compared with the results obtained by Oen and Robinson[18] using a continuous slowing-down model. Their calculation used the LSS inelastic energy loss model[16] and an approximation[19] to the elastic stopping cross section developed by Lindhard *et al.*[20] The dashed curve in Fig. 10 was obtained from Oen's and Robinson's calculation with the screening length used in the MARLOWE calculations and with the final energy $E_c/2$. Because the times are additive in the analytical model, changes in the final energy correspond to moving the dashed curve vertically in the figure: Changing the final energy to E_c, for example, reduces the slowing-down time by 7 fs everywhere. More importantly, although the same screening length was used, the potentials were different in the two calculations. The energy-dependent potential corresponding to the Lindhard differential scattering cross section has been deduced[21] using an inversion procedure of Firsov's.[22] At the highest energies in the present calculation, this potential is somewhat less repulsive than is the Molière potential, while at the

lowest energies it is somewhat more repulsive. These differences correspond qualitatively to the fact that the analytical slowing-down times are greater than the MARLOWE results for high energies, but are less for low energies.

Figure 11 shows the radial range and slowing-down time distributions evaluated for 10-keV primaries. Both functions are much less skewed than are those for the crystalline targets and there is no sign of the long tails which are the signature of channeling. The slowing-down time distribution is very nearly Gaussian. The mean values of both distributions lie quite close to the modes (most probable values), unlike the situation for the crystalline targets. The joint distribution also shows only the appearance of a two-dimensional Gaussian distribution. Thus, the appearance of the distributions for the amorphous medium confirms the identification of channeling in the crystalline distributions.

VI. CONCLUSION

The work reported here shows how evaluations of significant times can be included in BCA calculations without altering the event-driven character of the model and without major impact on the computational efficiency. It therefore appears feasible to treat the collisions in a complete cascade calculation in proper time order, rather than in the velocity order or other order that has been used before. The broad range of slowing-down times displayed in Figs. 6–9 already suggest that reordering the collisions may have significant consequences: Since cascades develop by generating mostly low-energy projectiles, many particles must stop long before the high energy recoils slow down completely and interferences between fast and slow particles may be important.

Finally, the slowing-down times for primary recoils allow some remarks to be made about the validity of separating collision cascade development into separate collisional and many-body phases. The mean slowing-down times, even at 10 keV, are short enough to separate the collisional phase reasonably cleanly from the direct effects of thermal vibrations, diffusion, and other many-body effects, which typically are concerned with times of a few hundred femtoseconds or more. However, as the distribution functions of Figs. 7 and 9 show, some particles take much more than the mean time to slow down, especially when channeling is important. Thus, at the very least, the "frozen" thermal displacement model which is often used in cascade calculations[1,8] may be unreliable. To say more than this requires extensive study of whole cascades.

ACKNOWLEDGMENTS

This research was sponsored by the Division of Materials Sciences, U.S. Department of Energy under Contract No. DE-AC05-84OR21400 with Martin Marietta Energy Systems, Inc.

[1]M. T. Robinson, in *Sputtering by Particle Bombardment I,* edited by R. Behrisch (Springer Verlag, Berlin, 1981), pp. 73–144.
[2]D. E. Harrison, Radiat. Eff. **70**, 1 (1983).
[3]J. R. Beeler, Jr., *Radiation Effects Computer Experiments* (North-Holland, Amsterdam, 1983).
[4]H. H. Andersen, Nucl. Instrum. Methods B **18**, 321 (1987).
[5]F. F. Abraham, Adv. Physics **35**, 1 (1986).
[6]T. Diaz de la Rubia, R. S. Averbach, R. Benedek, and W. E. King, Phys. Rev. Lett. **59**, 1930 (1987).
[7]Y. Yamamura, Nucl. Instrum. Methods B **33**, 493 (1988); Nucl. Instrum. Methods **194**, 515 (1982).
[8]M. T. Robinson and I. M. Torrens, Phys. Rev. B **9**, 5008 (1974).
[9]M. Hou and M. T. Robinson, Nucl. Instrum. Methods **132**, 641 (1976).
[10]M. T. Robinson, J. Appl. Phys. **54**, 2650 (1983).
[11]M. T. Robinson, Phys. Rev. B **27**, 5347 (1983).
[12]M. T. Robinson, *User's Guide to* MARLOWE *(Version 12),* describes a version of the program which is available from the National Energy Software Center, Argonne National Laboratory, Argonne, Illinois 60439, and from the Radiation Shielding Information Center, Oak Ridge National Laboratory, Oak Ridge, Tennessee 37831–6362. The greatly modified version of the program used in the present work is designated Version 12.5.
[13]H. Goldstein, *Classical Mechanics* (Addison-Wesley, Reading, Massachusetts 1959), pp. 58–89.
[14]M. T. Robinson and O. S. Oen, Phys. Rev. **132**, 2385 (1963).
[15]M. T. Robinson, U.S. Atomic Energy Commission Report ORNL-4556, 1970.
[16]J. Lindhard, M. Scharff, and H. E. Schiott, K. Dan. Vidensk. Selsk. Mat. Fys. Medd. **33**, No. 14 (1963).
[17]P. Jung, Phys. Rev. B **23**, 664 (1981).
[18]O. S. Oen and M. T. Robinson, J. Appl. Phys. **46**, 5069 (1975).
[19]K. B. Winterbon, P. Sigmund, and J. B. Sanders, K. Dan. Vidensk. Selsk. Mat. Fys. Medd. **37**, No. 14 (1970).
[20]J. Lindhard, V. Nielsen, and M. Scharff, K. Dan. Vidensk. Selsk. Mat. Fys. Medd. **36**, No. 10 (1968).
[21]M. T. Robinson, in *Radiation-Induced Voids in Metals,* AEC Symposium Series 26, edited by J. W. Corbett and L. C. Ianiello, (U.S. Atomic Energy Commission, Oak Ridge, Tennessee, 1972), pp. 397–428.
[22]O. B. Firsov, Zh. Eksp. Teor. Fiz. **24**, 79 (1953); see also J. B. Keller, I. Kay, and J. Shmoys, Phys. Rev. **102**, 557 (1956); W. H. Miller, J. Chem. Phys. **51**, 3631 (1969).